Evaluation of iron ore concentrate and micropellets as potential feed for sinter production

Thato Nkogatse [1], Andrie Garbers-Craig [1*]

1 Centre of Pyrometallurgy, Department of Materials Science and Metallurgical Engineering, University of Pretoria, Pretoria, South Africa

* Corresponding author: andrie.garbers-craig@up.ac.za

Evaluation of iron ore concentrate and micropellets as potential feed for sinter production

The use of iron ore concentrate and micropellets as sinter feed was evaluated. Five mixtures containing different proportions of concentrate and micropellets, together with iron ore fines, were granulated and sintered in a pilot scale sinter plant.

It was found that the addition of iron ore concentrate and / or micropellets to the sinter feed resulted in a significant increase in permeability of the granulated bed, but a large drop in sinter production rates. Although the introduction of iron ore concentrate and / or micropellets to the sinter mixture did not significantly impact sinter strength or reducibility (as measured through tumble - (TI) and reducibility indices (RI)), it severely impacted on their strengths during reduction (as measured through $RDI_{-3.5\ mm}$ and $RDI_{-0.5\ mm}$). The introduction of iron ore concentrate and micropellets resulted in a general increase in the amount of fines that form during reduction, exceeding the maximum acceptable levels ($RDI_{-0.5mm}$ maximum 5%) set by industry. Sinters containing high amounts of micropellets experienced a more severe degradation than the concentrate-rich sinters. It is therefore more viable to use iron ore concentrate in the sinter feed as higher production costs are associated with the production of micropellets. Sinters produced through concentrate addition also generate less fines on reduction.

1.   Introduction

Over 70% of steel is produced from iron ore (Poveromo, 2010, 2018). Iron ore is therefore a key component in the production of steel. The availability of high-grade iron ore is however diminishing and the use of concentrate is on the rise. In South Africa the advancement of iron ore beneficiation technology has allowed for the upgrading of the previously discarded slime and the production of a hematite concentrate (Mbele, 2012). Since iron ore concentrate comes from complex beneficiation processes, it is very fine and cannot be used directly in the blast furnace due to permeability and clogging concerns (Lwamba and Garbers-Craig, 2008, Pal *et al*., 2013; Pettersson *et al.*, 2015). It is therefore necessary to agglomerate the fine ore before it is charged into the blast furnace. This is done through sintering or pelletization, depending on the particle size distribution of the fines. Materials selected for sintering typically range in size from 0.1 mm to 8 mm whilst pelletization requires ultra-fine ore typically less than 75 μm (Eisele and Kawatra, 2003; Mbele, 2012; Poveromo, 2010; Mežibrick *et al.*, 2019). Iron ore sintering is currently the most utilized agglomeration process with a majority of blast furnaces allocating over 70% iron ore burden to sinter, 20% to pellets and 10% ore lumps (Lu, 2015). Sinter is produced when a mixture of fine iron ore, coke breeze, lime or limestone and dolomite, is rapidly heated for 2 – 4 minutes to temperatures of ~ 1300°C, after which it is cooled in air (Webster *et al.*, 2014). At high temperatures this mixture partially melts and upon cooling different phases crystallize and bond the structure to form a strong agglomerated mass (Umadevi *et al.*, 2011).

Fine iron ore can also be used in iron ore micropellets. These micropellets are produced by balling a mixture of iron ore concentrate and binders to form spherical particles with diameters of -5 mm +1 mm. Similar to the pelletization process, it is required that the particle size distribution of the feed be such that 80% of the material passes 200 mesh (74 microns) and have a minimum surface area of 900 cm^2/g (Roshan *et al.*, 2018).

Despite a coarser particle size distribution compared to the iron ore concentrate, the top size of iron ore micropellets is still smaller than the bottom size of iron ore generally accepted in the blast furnace. A significant amount of work is therefore being undertaken to assess the viability of utilizing iron ore micropellets as feed to the sinter making process (Pal *et al.*, 2013; Pal *et al.*, 2015; Pal, 2019; Nyembwe *et al.*, 2016; Roshan *et al.*, 2018).

The aim of this work was to assess the viability of using mixtures of Northern Cape iron ore concentrate and micropellets as feed for sinter making. This was done by analysing the permeability and granulation efficiency of the granulated mixtures, as well as the structure, mineralogy, properties and production rates of the produced sinter.

2. Materials and Methods

2.1. Preparation of raw material mixtures

The raw materials used in this study included iron ore fines (from two mines located in the Northern Cape, South Africa), lime, dolomite, coke, iron ore concentrate (particle size distribution of 0.32-955 µm with 99 % passing 0.5 mm) and iron ore micropellets (MP). The micropellets were constituted from concentrate, which implies that the chemical compositions of the concentrate and micropellets were similar. Corn starch (1 mass%) was used as binder during the production of the micropellets, while 0.1 mass% Acronal® paint was added to limit water absorption during granulation. The corn starch was prepared by mixing it with water (10% solids), heating it to 85°C, and then adding it hot to the raw material mixture, together with the Acronal. After pelletisation the micropellets were not fired but only dried naturally to minimise cost. Pellets in the -5 mm +1 mm size range, with a drop number of 6, were used in the sinter mixtures.

The chemical compositions of the dried raw materials are shown in Table 1. These raw materials were used to constitute five sinter mixtures containing different ratios of iron ore concentrate to micropellets. Compositions of the sinter mixtures as well as particle size distributions of each mixture before granulation are shown in Tables 2 and 3 respectively. The lime and coke addition was varied according to the amount of return fines used.

[Tables 1- 3 near here]

2.2. Granulation process

Granulation is carried out to produce a sinter feed consisting of granules (also called pseudo-particles) with a narrow granule size distribution in order to enhance the permeability of the sinter bed as well as the productivity of the sinter plant. For each test, a 80 kg sample (which included all the raw materials) was charged into a mixing drum where it was agitated for a total of 2 minutes whilst the required moisture was added. The agitated mixture was then fed into a granulation drum (0.5 m in diameter and 1 m in length). Granulation was done for a total of 2.5 minutes at 20 rpm, which was followed by feeding the sinter pot through a conveyor belt. One kilogram of the wet sample was taken for measurement of the granule size distribution and determination of the mechanisms through which layering occurred during granulation.

2.3. Permeability of the granulated bed

The permeability of the granulated bed was measured at 4 - 6% moisture additions in 0.5% increments. For the base case mixture however, permeability was measured from 3.25% moisture as maximum permeability was not observed in the 4 – 6% moisture

range. A similar approach was followed for the 10% MP mixture where 5.25% moisture was tested in order to determine the maximum permeability. The granulated mixtures were randomly charged into a permeameter (Figure 1) to create a bed 535 mm in height, on top of a 1 mm screen that served as support for the bed. A venturi system was then sealed securely on top of the permeameter and a suction fan, which consisted of a manual valve to control pressure across the bed, at the bottom of the permeameter. Air was drawn across the bed at 1000 mmH$_2$O suction pressure, while pressure was measured in the venturi, above and below the bed. The pressure in the venturi was used to calculate the flow rate (Q), which was then used to calculate the permeability of the bed in JPU, using Equation 1. The permeability of each mixture was measured twice.

[Figure 1 near here]

$$JPU = \frac{Q}{A} \left(\frac{H}{\Delta P}\right)^{0.6} \tag{1}$$

Where:

JPU = Japanese Permeability Unit

Q = air flow rate (m^3/min)

A = cross sectional area (m^2)

H = height of packed bed (mm)

ΔP = pressure drop across the bed (mm H$_2$O)

2.4. Granule size distribution of the granulated mixture

The granule size distribution (GSD) was measured using the wet granulated sample from the permeability test. To avoid breakage, the granules were manually sieved without the use of vibration. The screen sizes used for the analysis were 4, 2, 1 and 0.5

mm respectively. Only mixtures with optimum moisture (maximum permeability) were analysed. The results from the GSD analysis were used to calculate the mean sizes of the granules after granulation (D), material transfer (S) and fines elimination efficiency (E_x) using the following equations:

$$D = \frac{100}{(\Sigma \frac{x_i}{d_i})} \qquad (2)$$

$$S = (\% < X \ mm)_{BG} - (\% < X \ mm)_{AG} \qquad (3)$$

$$E_X = 100 * \frac{S}{S'} \qquad (4)$$

Where

D = mean granule size (mm)

x_i = mass % of granules of size fraction d_i

d_i = screen aperture (mm), mean granule diameter of size fraction i

S = material transfer (%)

X = screen size at which there is neither loss nor gain (mm)

$(\% < X \ mm)_{BG}$ = mass fraction less than X mm before granulation

$(\% < X \ mm)_{AG}$ = mass fraction less than X mm after granulation

S' = $(\% < X \ mm)_{BG}$

Ex = material transfer efficiency (%)

2.5. Production of sinter

The bench scale sinter pot tests were conducted at the Anglo American Value-In-Use facility located in Gauteng, South Africa. The sinter pot used in this study was a cylindrical pot with 320 mm internal radius and height of 550 mm (Figure 2). Prior to feeding the granulated material into the sinter pot, a 50 mm hearth layer was placed at the bottom of the pot in order to support the sinter bed. The effective bed height was therefore 500 mm. After feeding the sinter pot to maximum capacity, a burner

connected to an LPG – air system was used to ignite the bed to 1050 $^{\circ}$C, whilst the suction valve was set to a 1000 mmH$_2$O pressure drop. When the thermocouple at the bottom of the bed reported the maximum temperature, the sintering process was stopped as this suggested that the flame front has passed through the bed (Umadevi *et al.*, 2011). The sinter cake was then left to cool to 25 $^{\circ}$C at 800 mmH$_2$O, after which it was dropped three times, followed by sieve analysis.

[Figure 2 near here]

2.6. Evaluation of microstructures

2.6.1. Micro-Focus X-Ray Tomography (MF-XRT)

MF-XRT was conducted on granulated material as well as sinter particles (-25 mm +16 mm) in order to analyse the layering mechanisms of granulation as well as the internal structures of the grains and sinter. This was done using a Nikon XT H 225L system at the Nuclear Energy Corporation of South Africa. Multiple 2D images were constituted and stacked together using CT Pro 3D software to reconstruct a 3D structure. The 3D structures were then analysed using VG-Studio 3.2 software.

2.6.2. Optical microscopy

A Nikon Eclipse ME600P optical microscope was used to study the microstructures of the produced sinters.

2.7. Mineralogy

The mineralogy of the produced sinter was studied using X-ray diffraction (XRD), reflected light microscopy and Scanning Electron Microscopy using Energy Dispersive

Spectrometry (SEM-EDS). XRD analysis was performed using a PANalytical X'Pert

Pro powder diffractometer in θ–θ configuration, fitted with a X'Celerator detector,

variable divergence and fixed receiving slits with Fe filtered Co-Kα radiation

(λ=1.789Å). Preparation of the samples was according to the standardized PANalytical

backloading system, which provides nearly random distribution of the particles. The

phases were identified using X'Pert Highscore Plus software. Quantification was done

using the Autoquan program which utilizes the Rietveld method.

2.8. Evaluation of sinter properties

2.8.1 Tumble Index

The resistance of the produced sinter to size degradation by impact and abrasion was

evaluated by measuring its tumble index according to the ISO 3271:2015 test procedure.

A 15 kg sample of the -40 mm +10 mm sinter size fraction was rotated for 200

revolutions in a tumbling drum at 20 rpm followed by sieve analysis using 6.3, 3.5 and

0.5 mm screens respectively. The tumble index was calculated using the +6.3 mm

fraction according to Equation 5:

$$TI(\%) = 100 * \frac{m_1}{m_0} \qquad (5)$$

Where m_1 is the mass of the +6.3 mm fraction whilst m_0 is the original mass.

2.8.2.   Reduction Disintegration Index (RDI)

The reduction disintegration index (RDI), which is a measure of the degree of size

degradation of the produced iron sinter when reduced under conditions similar to those

in the low-temperature reduction zone of a blast furnace, was evaluated according to the

ISO 4696-1:2015 standard. Sinter particles from the -12.5 mm +10 mm size fraction

was reduced at 500°C in an atmosphere consisting of 20% CO_2, 20% CO, 2% H_2 and 58% N_2. After one hour the test sample was cooled to a temperature below 100°C and tumbled in a tumbling drum for 300 revolutions at 25 rpm. The sample was then screened through 6.3, 3.5 and 0.5 mm sieves respectively. Equations 6 to 8 were used to calculate the RDIs for the respective size fractions.

$$RDI_{-6.3} = \left(1 - \left(\frac{m_1}{m_0}\right)\right) * 100 \tag{6}$$

$$RDI_{-3.5} = \left(\frac{m_0 - (m_1 + m_2)}{m_0}\right) * 100 \tag{7}$$

$$RDI_{-0.5} = \left(\frac{m_0 - (m_1 + m_2 + m_3)}{m_0}\right) * 100 \tag{8}$$

Where

m_o = mass of sample after reduction before tumbling (in grams)

m_1 = mass of 6.3 mm oversize (in grams)

m_2 = mass of 3.5 mm oversize (in grams)

m_3 = mass of 0.5 mm oversize (in grams).

2.8.3. Reducibility Index

The reducibility index (RI) which assesses the reduction behaviour of iron ore burden materials in the middle zone of the blast furnace, was evaluated according to the ISO 4695-2015 procedure. A test portion of the -12.5 mm +10mm size fraction was reduced isothermally at 950°C in a gas mixture of 40% CO and 60% N_2. The test portion was weighed at specified time intervals and the mass loss calculated. The RI was calculated according to Equation 9:

$$RI(\%/min) = \left(\frac{m_0 - m_1}{m_0 * \Delta t}\right) * 100 \tag{9}$$

Where

m_o = initial sample mass (g)

m_1 = final sample mass (g)

Δt = reduction time (min)

2.9. Production rate of sinter

The production rate is a techno-economic indicator of the productivity or capacity of a sinter plant. It is calculated from the mass of sinter produced (excluding the -5mm fraction and the hearth layer used), the area of the hearth and the burn-through time according to Equation 10.

$$P = \frac{m_{total} - m_{-5mm} - (m_{hearth_{in}} - m_{hearth_{out}})}{A * t} \qquad (10)$$

Where

P   = productivity ($t/m^2/day$)

m_{total} = total mass of sinter produced (t)

m_{-5mm} = mass of the -5 mm fraction (t)

$m_{hearth,in}$ = mass of hearth layer added onto the strand (t)

$m_{hearth,out}$ = mass of hearth layer recovered (t)

A   = area of the grate (m^2)

t   = sintering time (day)

The different size fractions were obtained from the drop test that the sinter cake was subjected to after it was discharged from the sinter pot. The +16 mm size fraction was used as the hearth layer, which was subtracted from the cake mass after the pot test.

3.   Results and Discussion

3.1.   *Granulated mixtures*

3.1.1. *Permeability*

All the raw material mixtures reached their maximum permeability at 5% moisture except

the base case and 10% MP mixtures. The maximum permeabilities of the base case and the

10% MP mixtures were at 3.50% and 5.25% moisture respectively. The maximum bed

permeability of the base case mixture was significantly lower than that of the concentrate

and / or micropellet – containing mixtures (30.0 JPU vs. 33.8 – 38.7 JPU, Figure 3). The

0% MP, 10% MP, 20% MP and 40% MP mixtures had similar maximum bed permeabilities

(33.8 – 35.4 JPU) except for the 30% MP mixture, which exhibited a significantly higher

permeability of 38.7 JPU.

[Figure 3 near here]

3.1.2. *Granulation potentials*

Before granulation the base case and 40% micropellet mixtures had the highest mean

particle size, while the mean particle size of the concentrate – micropellet mixtures

increased with increasing micropellet content (Figure 4). After granulation however, the

mixture containing a higher amount of concentrate but also some micropellets (10%

MP) had the biggest mean granule size and the 40% micropellet mixture the smallest

(Figure 4). Increasing the micropellet content in the granulation mixture did not result in

increasing mean granule sizes. The mixture that contained concentrate only (0% MP)

also had a smaller mean granule size than the base case, 10% MP and 30% MP

mixtures, which indicates that there is a limit beyond which further addition of fines to

the raw material mixture no longer contribute to granule growth. Material transfer

decreased with an increase in micropellet content and an accompanying reduction in concentrate content (Figure 5). Material transfer efficiencies (Ex) were generally higher for mixtures containing higher amounts of concentrate as compared to those containing higher micropellet contents (0, 10 and 20 % vs. 30 and 40 % MP mixtures) (Table 4). The low transfer efficiency of the 30% MP mixture is mainly due to insufficient amounts of adhering fines (-0.5 mm particles) which could facilitate attachment. It was unexpected to find that the granulation efficiency of the 40% MP sample was higher than that of the 30% MP sample, although there was no concentrate added to the 40% MP mixture. This is presumably due to more micropellets that deformed and disintegrated in the 40% MP sample. Deformed micropellets could more easily attach to each other than spherical micropellets, while adhering fines could also more easily attach to deformed micropellets than to spherical micropellets. Although there was more transfer of material from the fine to the coarser size class, the amount of concentrate in the 30% MP mixture was not sufficient to maintain strong granules.

[Table 4 near here]

[Figure 4 near here]

[Figure 5 near here]

3.1.3.   MF-XRT analysis of granules

It was observed that most of the micropellets do not appear spherical after granulation. Micropellets obtained from the 30% MP sinter mixture also exhibited some degree of breakage, as can be seen in Figure 6. The lack of sphericity is presumably the result of deformation and breakage of the micropellets due to water uptake during granulation as well as the granulation process itself.

[Figure 6 near here]

Various layering mechanisms were observed in the pseudo-particles that formed in the different granulated mixtures. Auto layering, which involves the adherence of fines to angular nuclei particles, was observed in all the samples. Coagulation of fines to form spherical lumps, similar to what is observed during pelletisation, was observed in samples that contained 0, 10, 20 and 30% micropellets. Adhesion of deformed micropellets was observed when the concentrate was completely replaced with micropellets (40% MP). Some adhering fines covered the granules that formed by the direct adhesion of micropellets.

3.2. Firing of micropellets without and with flux addition

Raw micropellets were fired without and with the addition of fluxes, using an infrared furnace, in order to assess whether the microstructural changes associated with the micropellets take place as a result of melt infiltration or not. Raw micropellets consist of a fine hematite-silica-based matrix, which contains coarse hematite aggregates and low concentrations of muscovite (Figure 7a and b). Pores of irregular shape and interconnected pores can be observed (Figure 7b). When the micropellets were fired in an infrared furnace, it sintered, appeared denser than the raw micropellets, while the pores were mostly pinched off, i.e. closed and spherical (Figure 7c). Secondary skeletal hematite particles could be observed in the fired micropellets, which indicates that reduction and re-oxidation of hematite occurred.

[Figure 7 near here]

When the micropellet was coated with a mixture of iron ore fines, fluxes and coke, sintering took place along the rim of the micropellet whilst the core remained unreacted (Figures 7d and 8). The fine pores in the rim suggest that there was not extensive melt

formation around the micropellet during sintering. The dense nature of the rim also suggests that there was some reduction along the surface of the micropellet. The amount of reducing gas reaching the unreacted part of the micropellet however decreased as the film became thicker, causing the core to remain unchanged. It can then be argued that similar to the coarse relict hematite particles, iron ore micropellets can only assimilate provided that there are sufficient adhering fines to partially melt during sintering. The breaking down of micropellets during granulation however also provides a mechanism by which they can be assimilated. Such breakdown however introduces fines which can negatively impact bed permeability.

[Figure 8 near here]

3.3.   Sinter produced

3.3.1. Sinter structures

3.3.1.1. MF-XRT

The structures that formed during sintering are shown in Figure 9. It can be seen that the sinter that contained a 40% iron ore concentrate (0% MP) exhibit a relatively denser structure compared to the sinter with higher proportions of micropellets. The fine concentrate facilitated agglomeration and the formation of a denser bonding phase with relatively fine pores. The 40% MP sinter shows a significant number of open pores. The base case sinter also has a dense appearance, which is presumably due to the slightly higher adhering fines (-0.5 mm) content before sintering, as compared to the 40% MP sample.

[Figure 9 near here]

3.3.1.2. Optical Microscopy

The differences between the microstructures of the produced sinters reflect the differences in the reactivities of the sinter beds due to differences in granule size distributions. The bonding matrix surrounding the coarse nuclei in the base case sinter is mainly characterised by the presence of SFCA and SFCA-I needles (Figure 10(a)). The microstructure depicting the role of iron ore concentrate is reflected in the 0% MP sinter (Figure 10(b)). Reaction between the coarse nuclei and the bonding structure is more extensive compared to the base case sinter, while glass and secondary phases are more pronounced in this bonding structure. The bonding matrix of the 40% MP sinter which contained no concentrate is also SFCA-I rich, but with less secondary hematite than in the 0% MP sample (Figure 10(d)). In the instance where iron ore concentrate and micropellets were added in equal quantities (20% MP, Figure 10(c)), a denser bonding matrix formed, similar to the base case sinter, with secondary hematite precipitating along the rim of the coarse relict hematite nuclei.

[Figure 10 near here]

3.3.2. Mineralogy

X-ray diffraction was used to quantify the crystalline sinter phases produced from each mixture (Figure 11). The amount of hematite increased slightly as the amount of micropellets increased. Magnetite showed a nearly opposite trend to that of hematite. Since the starting ore did not contain any magnetite, the magnetite found in the sinter is due to the conversion from hematite as well as precipitation from the melt. The increase in hematite content and decrease in magnetite content with increasing amount of micropellets can be explained by the increase in mean particle size before granulation.

16

This resulted in a decrease in surface contact between the coke, fluxes and hematite in the micropellets.

The quantity of silico-ferrite of calcium and aluminium (SFCA, $Ca_{2.3}Mg_{0.8}Al_{1.5}Fe_{8.3}Si_{1.1}O_{20}$) decreased as a result of increasing amounts of micropellets, while the amount of SFCA-I ($Ca_{3.18}Fe_{15.48}Al_{1.34}O_{28}$) increased. The total amount of SFCA (SFCA and SFCA-I) of the base case sinter was the highest, followed by the sinter that only contained concentrate. The sinters that contained different amounts of micropellets had similar amounts of total SFCA. The base case sinter contained the highest amount of SFCA-I while the sinter that only contained concentrate contained the lowest amount of SFCA-I, but the highest amount of SFCA. The amount of larnite (β-Ca_2SiO_4) also decreased with increasing amounts of micropellets. The 10% MP sinter, which had the biggest mean granule size, had the highest amount of magnetite, lowest amounts of SFCA and larnite and also low amounts of SFCA-I.

According to Webster et al. (2014) SFCA-I can form prior to melt formation as a result of the reaction between Fe_2O_3, calcium ferrites and SiO_2, and decompose upon melt formation into Fe_2O_3 and melt. Although upon cooling SFCA-I forms again, it is short lived as further reaction with the melt leads to the formation of SFCA. This is particularly important because the 0% MP sinter contained the highest amount of SFCA. This suggests that the granules formed from this mixture were sufficiently fluxed to allow for melt formation and the cooling was sufficiently slow to allow for the crystallization of SFCA. Based on the increasing SFCA-I as the micropellet content was increased, it can be argued that the degree of melt formation decreased. This can also be seen from the decrease in larnite which normally precipitates from silica rich parts of the melt (Mulvaney, 1987; Hapugoda et al., 2016). Since SFCA-I is mostly stable during the heating stage, those sinters containing high concentrations of SFCA-I suggest

that not a large amount of melt remained.

[Figure 11 near here]

3.3.3. Sinter properties

3.3.3.1. TI, RDI and RI

The tumble indices of sinters that contain different proportions of iron ore concentrate and micropellets are similar to that of the base case sinter and similar to each other (Figure 12). The cold sinter strengths (TI) do not directly correspond to the SFCA-I content of the sinters, as increasing amounts of SFCA-I were present in the sinters as the micropellet content increased, although their cold strengths were similar. While the base case and 0% MP sinters had denser structures (as determined by MF-XRT) their tumble indices also did not differ from those of the other less dense sinters.

The $RDI_{-3.5\ mm}$ and $RDI_{-0.5\ mm}$ increased significantly as the micropellet content of the sinter mixture increased (Figures 18 and 19). This implies that sinters with higher proportions of micropellets tend to produce more fines on reduction, as compared to sinters containing higher proportions of concentrate. In general, sinters produced from concentrate and micropellets formed larger amounts of fines, compared to the base case sinter, and exceeded the acceptable limits of 30% and 5% for $RDI_{-3.5\ mm}$ and $RDI_{-0.5\ mm}$ respectively. The increasing amounts of fines produced on reduction indicate that bonds that were established in the concentrate – micropellet containing sinters were not strong enough to accommodate the volumetric changes associated with the reduction of hematite.

The effect of iron ore concentrate and micropellet addition on the reducibility of the sinter was also studied (Figure 20). The RI of the sinters that contained concentrate and micropellets did not differ significantly from that of the base case sinter, with RI values ranging between 1.5 and 2 %min^{-1}, which are all above the industry acceptable level of 1 %min^{-1}.

[Figure 12 near here]

[Figure 13 near here]

[Figure 14 near here]

[Figure 15 near here]

3.3.4. Production rate

The effect of the addition of micropellets and concentrate on the production rate was significant (Figure 16). The base case sample showed significant shorter sinter times compared to all the sinters that contained concentrate and / or micropellets.

[Figure 16 near here]

5. Conclusions

The main focus of this study was to assess the viability of utilizing iron ore concentrate and micropellets as sinter feed. It was established that:

- During granulation micropellets can deform, disintegrate or maintain their smooth and spherical nature. Deformation is presumably due to water addition during granulation, as well as to the granulation process itself. The micropellets that deformed took part in auto layering during granulation, those that disintegrated formed part of the fines, while those that maintained their shape contributed little to the formation of granules.

- Micropellet addition to the sinter mixture does not result in a significant increase in mean granule size after granulation. Although significant material transfer is facilitated by the use of large quantities of concentrate, maximum granule growth was achieved when both concentrate and micropellets were used (30% concentrate and 10% MP).

- The addition of iron ore concentrate and micropellets to sinter mixtures resulted in a considerable increase in permeability of the granulated bed, but in a significant drop in sinter production rates.

- The base case sinter as well as the sinter that contained 40% concentrate (0% MP)) had the highest densities. These sinters had the highest total SFCA concentrations.

- The replacement of 40 mass% of the iron ore fines in the sinter mixture with either iron ore concentrate, micropellets or mixtures of concentrate and micropellets do not significantly affect the reducibility and tumble indices of the sinter, but significantly reduce the reduction disintegration indices to unacceptable levels of fines production. Sinters containing high amounts of micropellets experience a more severe reduction degradation that the concentrate-rich sinters.

- The use of naturally dried micropellets as a sinter raw material in the proportions used in this study adds no benefits to the properties of the produced sinter. Since the role played by the micropellets in the sinter mixtures was not significantly different from that of the fine iron ore concentrate, the use of iron ore concentrate as a sinter feed is therefore more viable due to its lower production cost.

Declaration of interest statement

The authors have no conflict of interest to declare.

References:

Eisele, T. C., and Kawatra, S. K., 2003, "A review of binders in iron ore pelletization." Mineral Processing and Extractive Metallurgy Review, 24, pp. 1–90.

Hapugoda, S., Lu, L., Donskoi, E., and Manuel, J.R., 2016, "Mineralogical quantification of iron ore sinter." Mineral Processing and Extractive Metallurgy IMM Transactions Section C, 125(3), pp. 156-164.

Lu, L., 2015, *Iron Ore*. 56th edn. Sawston, Cambridge: Woodhead Publishing.

Lwamba, E., and Garbers-Craig, A. M., 2008, "Control of the grain size distribution of the raw material mixture in the production of iron sinter." *Journal of the Southern African Institute of Mining and Metallurgy*, 108(5), pp. 293–300.

Mbele, P., 2012, "Pelletizing of Sishen concentrate." *Journal of the Southern African Institute of Mining and Metallurgy*, 112, pp. 5–7.

Mežibrick, R., Fröhlichova, M., Findorák, R., and Goettgens, V.S., 2019, "Ore Assimilation and Secondary Phases by Sintering of Rich and High-Gangue Iron Ores." *Minerals*, 9(128), pp. 1-25.

Mulvaney, R. 1987, "Iron Ore Sinter in the Analytical Transmission Electron Microscope." Mineralogical Magazine, 51, pp. 61-69.

Nyembwe, A. M., Cromarty, R. D., and Garbers-Craig, A. M., 2016, "Prediction of the granule size distribution of iron ore sinter feeds that contain concentrate and micropellets.", *Powder Technology*, 295, pp. 7–15.

Pal, J., Ghorai, S., Venkatesh, P., Goswami, M. C., Bandyopadhyay, D., and Ghosh, S., 2013, "Development of fluxed micropellets for sintering utilising iron oxide waste fines.", *Ironmaking & Steelmaking*, 40(7), pp. 498–504.

Pal, J., Ghorai, S., and Das, A., 2015, "Development of carbon composite iron ore micropellets by using the microfines of iron ore and carbon-bearing materials in iron making." *International Journal of Minerals, Metallurgy and Materials*, 22(2), pp. 132-140.

Pal, J., 2019, "Innovative Development on Agglomeration of Iron Ore Fines and Iron Oxide Wastes.", *Mineral Processing and Extractive Metallurgy Review*, 40(4), pp. 248–264.

Patrick, T. R. C., and Lovel, R. R., 2001, "Leaching Dicalcium Silicates from Iron Ore Sinter to Remove Phosphorus and Other Contaminants." *ISIJ International*, 41(2), pp. 128–135.

Pettersson, M., Sikström, P., and Ritz, V., 2015, "Effect of magnetite , hematite and pellet screenings as sinter feed."

https://www.lkab.com/en/SysSiteAssets/documents/kund/2016-effect_of_magnetite_hematite_and_pelletscreenings_as_feed_in_sinter_pr.pdf

Poveromo, J. J., 2010, "5th International Congress on the Science and Technology of Ironmaking." *Steel Times International*, 34(1), pp. 28–30.

Poveromo, J2018 SME Annual Conference and Expo and 91st Annual Meeting of the SME-MN Section 2018-February, pp. 1–7.

Roshan, V., Kumar, K., Kumar, R., and Nageswara Rao, G. V. S., 2018, "Preparation of Iron Ore Micro-pellets and Their Effect on Sinter Bed Permeability.", *Transactions of the Indian Institute of Metals*. Springer India, 71(9), pp. 2157–2164.

Umadevi, T., Brahmacharyulu, A., Roy, A. K., Mahapatra, P. C., Prabhu, M., and Ranjan, M., 2011. "Influence of Iron Ore Fines Feed Size on Microstructure, Productivity and Quality of Iron Ore Sinter.", *ISIJ International*, 51(6), pp. 922–929.

Webster, N. A. S., Pownceby, M. I., Madsen, I. A. N. C., Studer, A. J., Manuel, J. R.,

and Kimpton, J. A., 2014, "Fundamentals of Silico-Ferrite of Calcium and Aluminum (SFCA) and SFCA-I Iron Ore Sinter Bonding Phase Formation : Effects of CaO : SiO$_2$ Ratio.", *Metallurgical and Materials Transactions B: Process Metallurgy and Materials Processing Science*, 45, pp. 2097–2105.

Table 1. Chemical compositions of the raw materials used

Material	Fe(tot)	FeO	Fe$_2$O$_3$	K$_2$O	Na$_2$O	CaO	MgO	MnO	Al$_2$O$_3$	SiO$_2$
Fines A[1]	63,8	0,27	91,81	0,15	0,01	0,00	0,02	0,26	2,45	5,02
Fines B[1]	65,2	0,27	93,86	0,21	0,07	0,17	0,02	0,05	1,20	4,14
Concentrate	66,3	0,10	95,64	0,21	0,01	0,11	0,03	0,05	1,34	2,50
Micropellets	66,3	0,00	95,79	0,21	0,01	0,11	0,03	0,00	1,34	2,51
RF[2]	58,7	2,03	79,87	0,22	0,03	9,05	2,81	0,25	1,67	4,07
Coke	1,35	0,93	9,54	1,43	0,71	5,27	1,97	0,22	23,97	55,95
Lime	0,49	0,73	0,44	0,55	0,00	94,61	2,05	1,08	0,27	0,27
Dolomite	0.97	0.0	2.59	0.04	0.00	56.03	37.48	1.56	0.19	2.12

[1] Fines obtained from two mines in the Northern Cape
[2] RF = Return fines, produced from sinters containing no concentrate nor micropellets

Table 2. Compositions of the dry sinter mixtures (mass%)

Material	Base Case[1]	0% MP	10% MP	20% MP	30% MP	40% MP
Fines A	24.37	15.98	16.07	15.61	15.50	15.12
Fines B	24.37	15.98	16.07	15.61	15.50	15.12
Concentrate	0.00	21.24	16.02	10.38	5.15	0.00
Micropellets	0.00	0.00	5.34	10.38	15.46	20.10
Return Fines[2]	31.73	27.87	27.46	29.51	30.01	31.73
Coke	4.32	4.59	4.62	4.49	4.46	4.35
Lime	7.19	5.81	5.84	5.68	5.64	5.50
Dolomite	8.03	8.54	8.59	8.35	8.29	8.08
Total	100.00	100.00	100.00	100.00	100.00	100.00

MP = Micropellets

[1] Typical sinter mixture used in a South African sinter plant, called the 'base case'

[2] For each mixture the return fines ratio was kept at 1

Table 3. Particle size distributions of the sinter mixtures before and after granulation
(mass%)

Size (mm)	Base Case		0% MP		10% MP		20% MP		30% MP		40% MP	
	Mass % BG	Mass % AG	Mass % BG	Mass % AG	Mass % BG	Mass % AG	Mass % BG	Mass % AG	Mass % BG	Mass % AG	Mass % BG	Mass % AG
+4	29.63	34.43	19.29	34.71	22.21	39.12	25.15	32.15	28.08	38.37	31.01	31.62
-4 +2	31.63	41.90	21.95	39.20	25.43	44.13	28.91	40.87	32.39	38.59	35.87	39.48
-2 +1	18.14	19.79	12.96	21.35	13.91	14.73	14.86	20.92	15.81	18.62	16.76	20.73
-1 + 0.5	6.99	3.62	4.86	4.62	4.86	1.95	4.86	5.95	4.86	4.13	4.86	7.12
-0.5	13.60	0.26	40.95	0.12	33.60	0.07	26.22	0.10	18.86	0.28	11.51	1.05
Total	100.00	100.00	100.00	100.00	100.00	100.00	100.00	100.00	100.00	100.00	100.00	100.00

Table 4: Granulation potentials of the base case and concentrate - micropellets

mixtures.

	D (BG)	D (AG)	X (mm)	S (%)	Ex (%)
Base Case	1.37	2.37	0.85	16.72	81.2
0% MP	0,79	2,30	0,5	40,82	99,68
10% MP	0,9	2,65	0,85	36,44	94,77
20% MP	1,04	2,22	0,5	25,03	95,45
30% MP	1,25	2,39	0,55	19,3	81,36
40% MP	1,54	2,07	0,45	10,46	90,9

BG = Before granulation
AG = After granulation
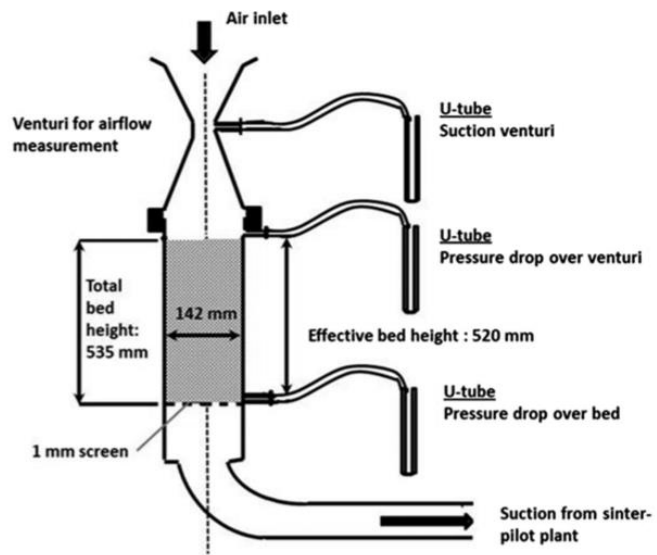
Figure 1: Experimental setup for the measuring of the JPU (Nyembwe et al,.2016).
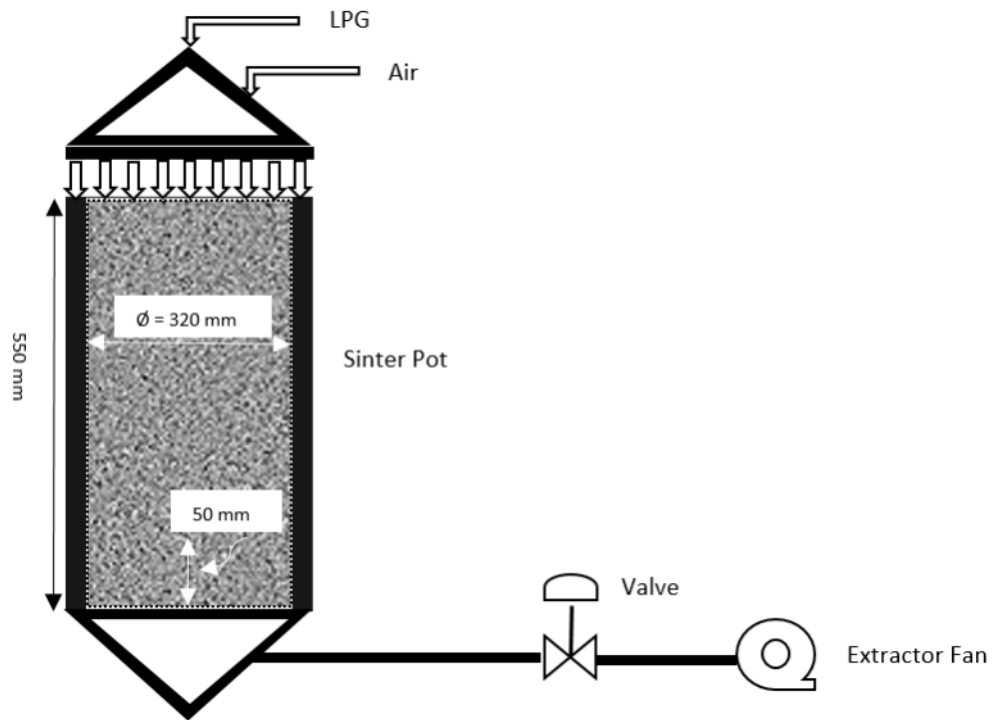
Figure 2. Schematic representation of the sinter pot test setup utilized at Anglo

American Value-In-Use.
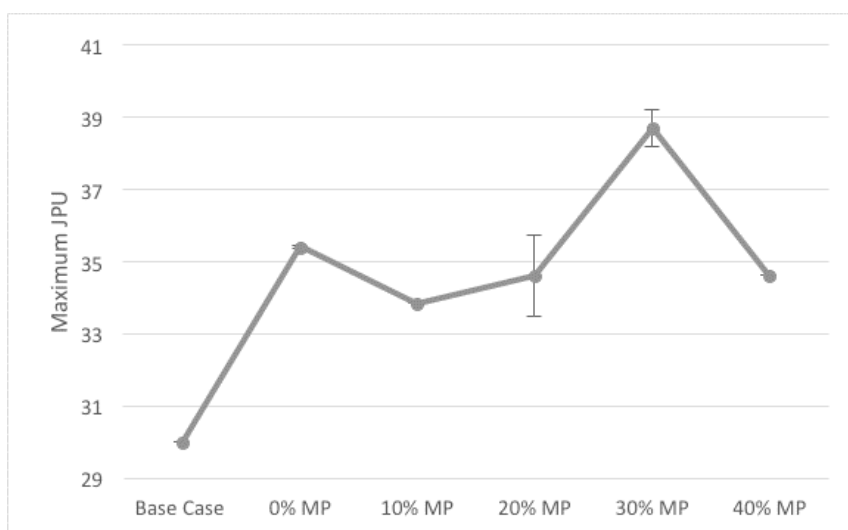
Figure 3: Maximum permeability as a function of micropellet to concentrate ratio. (Absence of error bars for some of the data points is due to little variability in the data.)
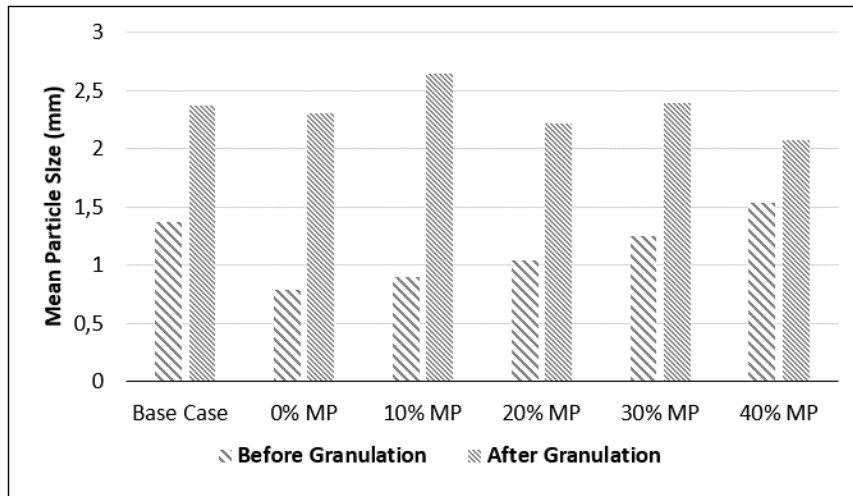
Figure 4. Mean particle size before ($D_{(BG)}$) and mean granule size after ($D_{(AG)}$) granulation as a function of micropellet and concentrate content.
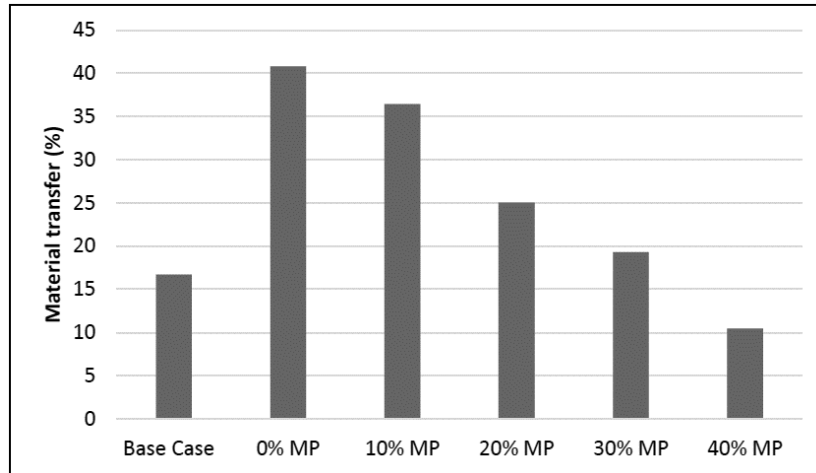
Figure 5. Material transfer (S) as a function of micropellet to concentrate ratio.
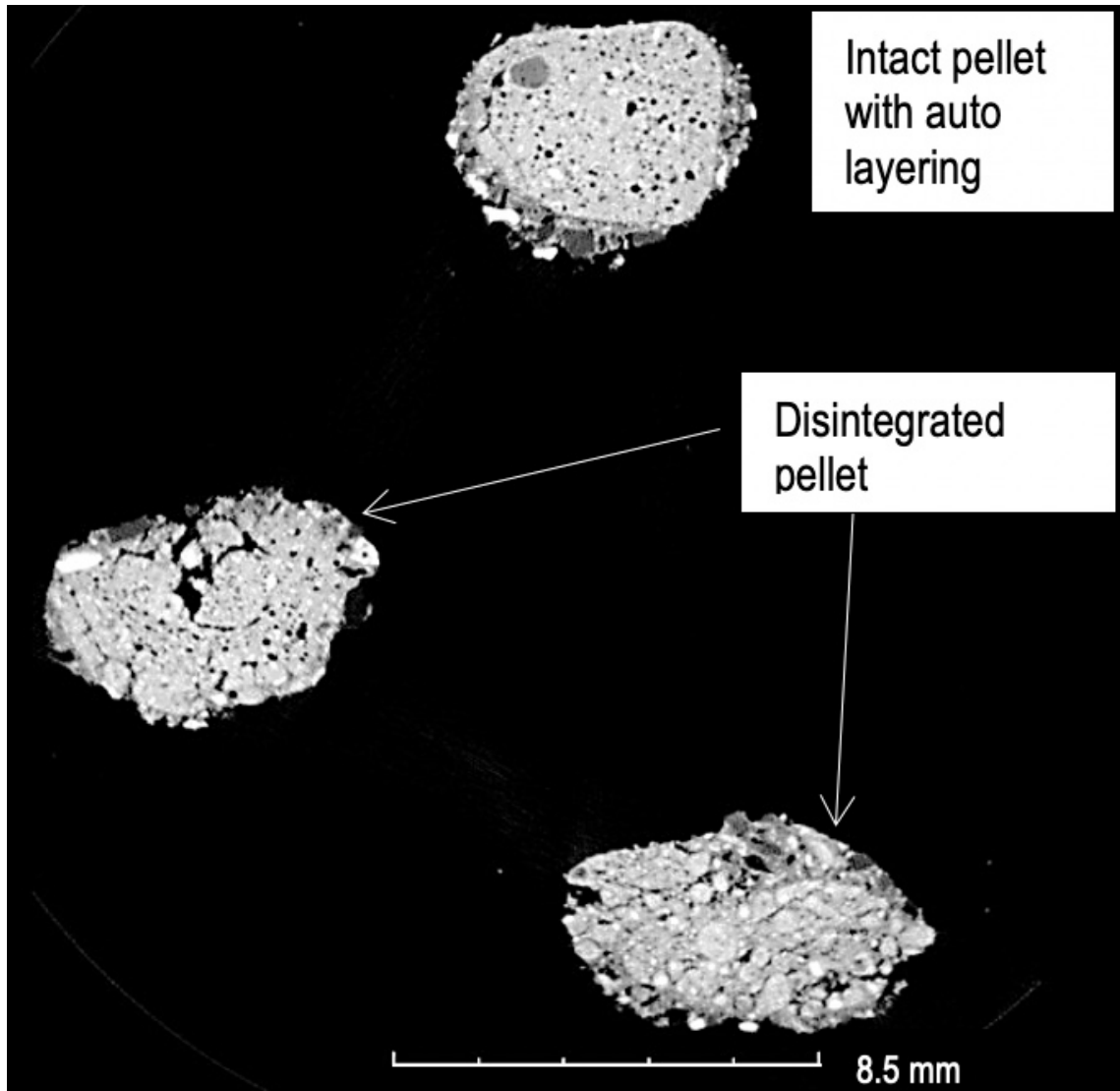
Figure 6: X-ray tomogram of micropellets obtained from the 30% MP mixture

at 5% moisture.
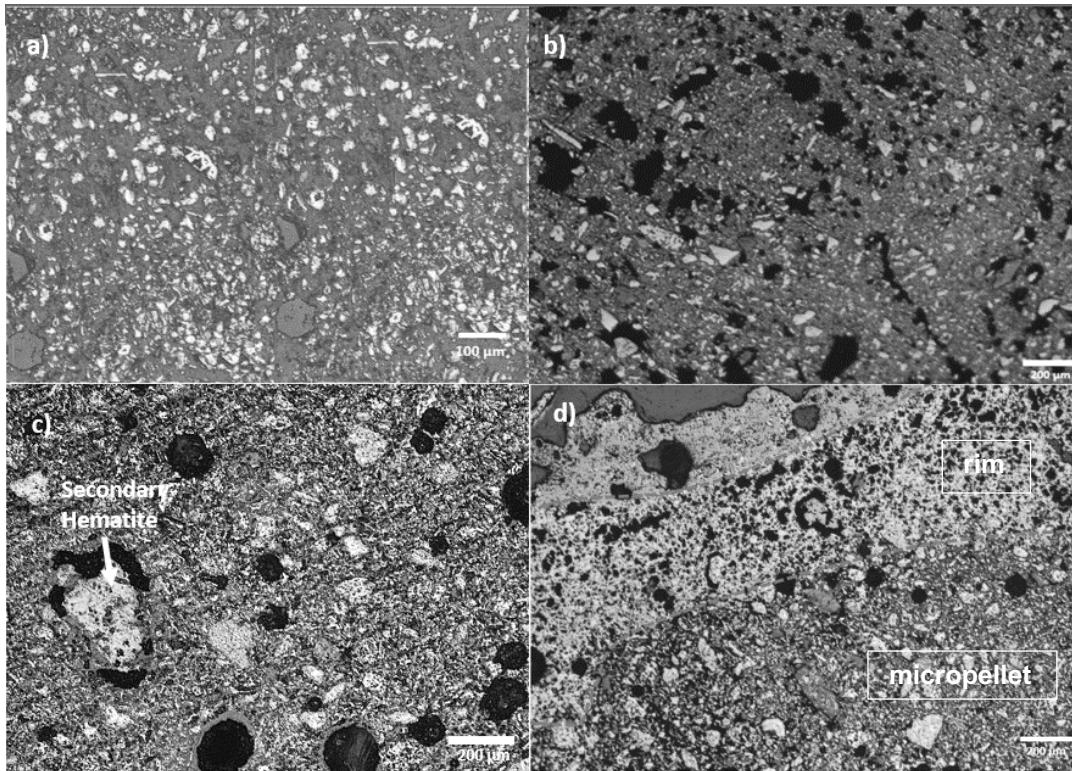
Figure 7: Optical micrographs of iron ore concentrate and micropellets.

a) Concentrate; b) Unreacted micropellet; c) Fired micropellet; d) Micropellet fired with fluxes.
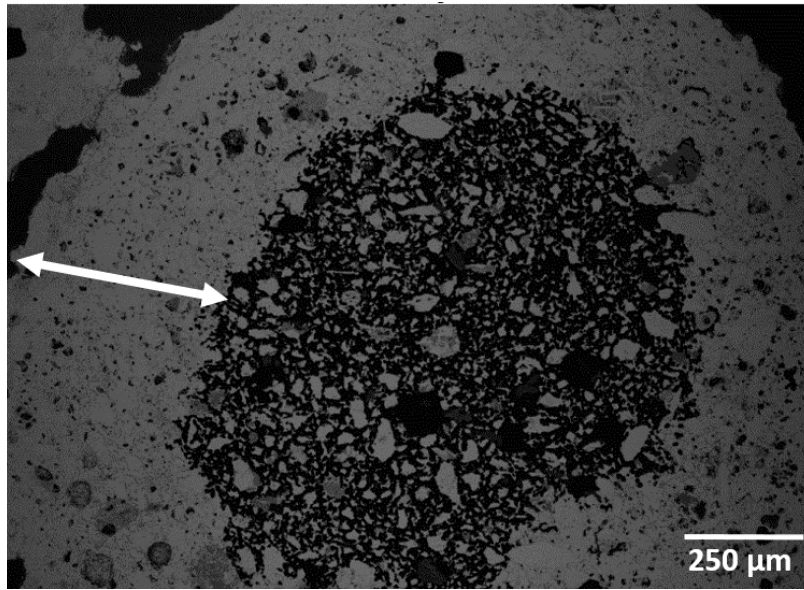
Figure 8: Backscatter electron image of a micropellet obtained from the 20%

MP sinter mixture showing a sintered layer surrounding an unreacted core
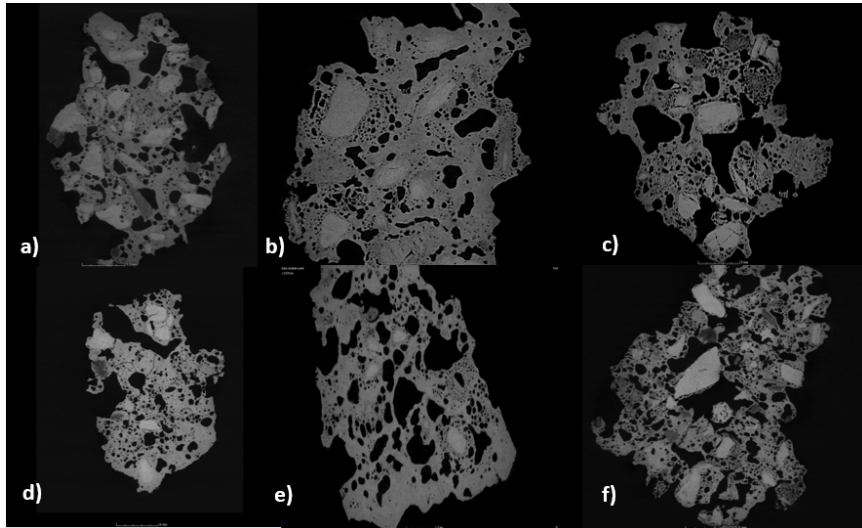
Figure 9: Cross sections of +16 mm sinter particles, reconstructed using MF-XRT.

a) Base case; b) 0% MP; c) 10% MP; d) 20% MP; e) 30% MP; f) 40% MP.
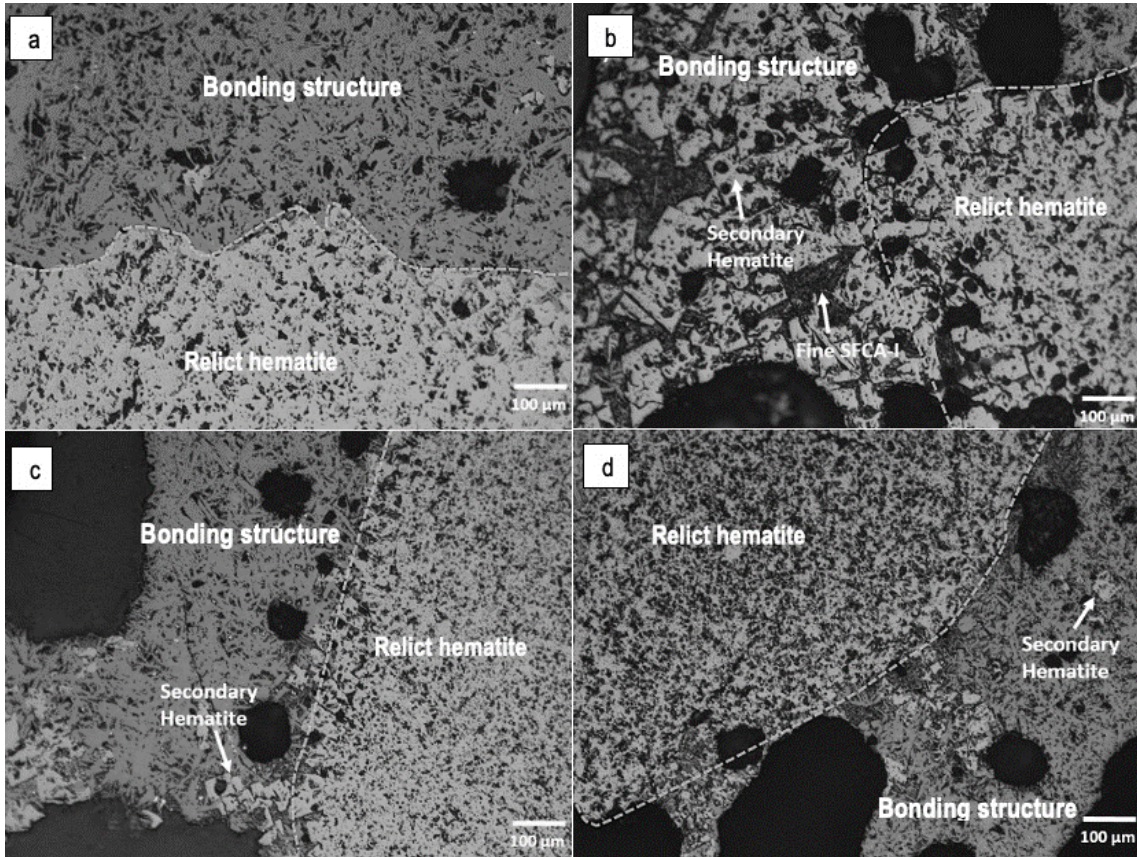
Figure 10: Optical micrographs of the (a) base case, (b) 0% MP, (c) 20% and (d) 40% MP sinters, indicating the attachment of the bonding structure to the relict particle.
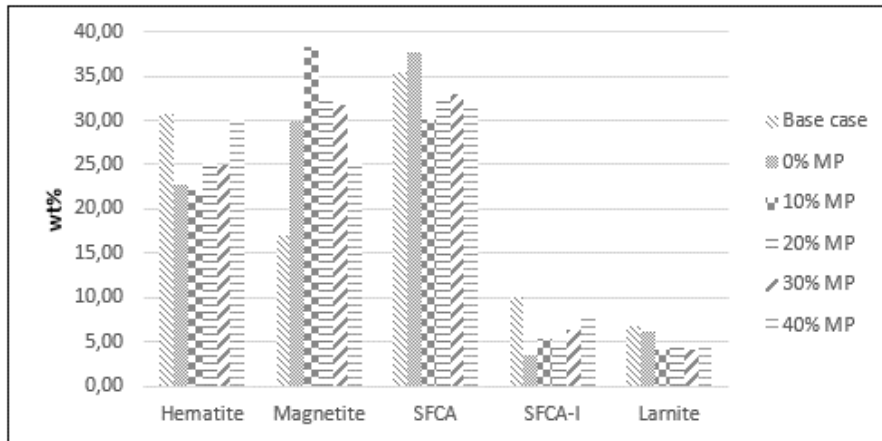
Figure 11: The relative proportions of the crystalline sinter phases formed in the

different sinter mixtures.
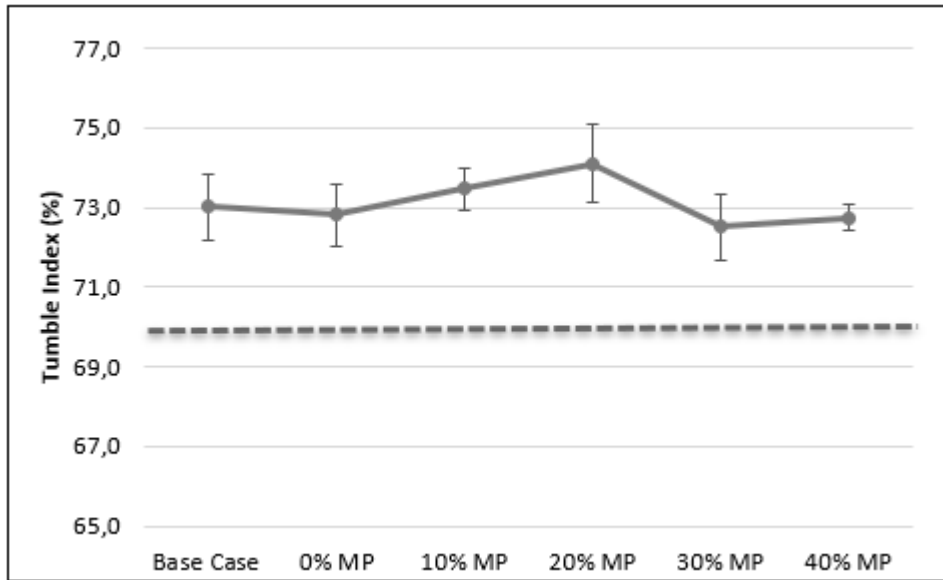
Figure 12: Tumble index as a function of concentrate and micropellet content.

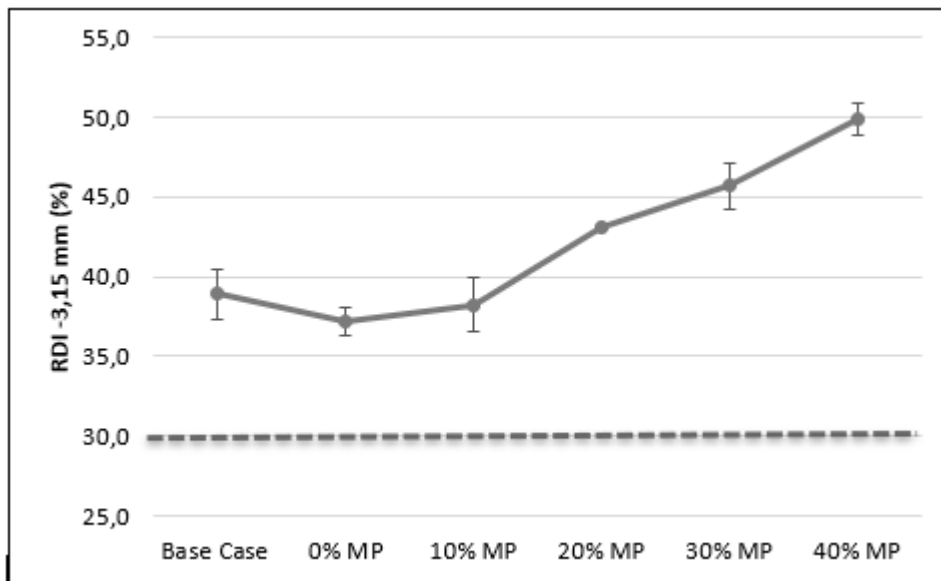(Minimum industry required value of 70% indicated on the diagram.)

Figure 13: Impact of micropellet and concentrate addition on -3.15 mm reduction disintegration index. (Maximum industry allowed value of 30% indicated on the diagram.)
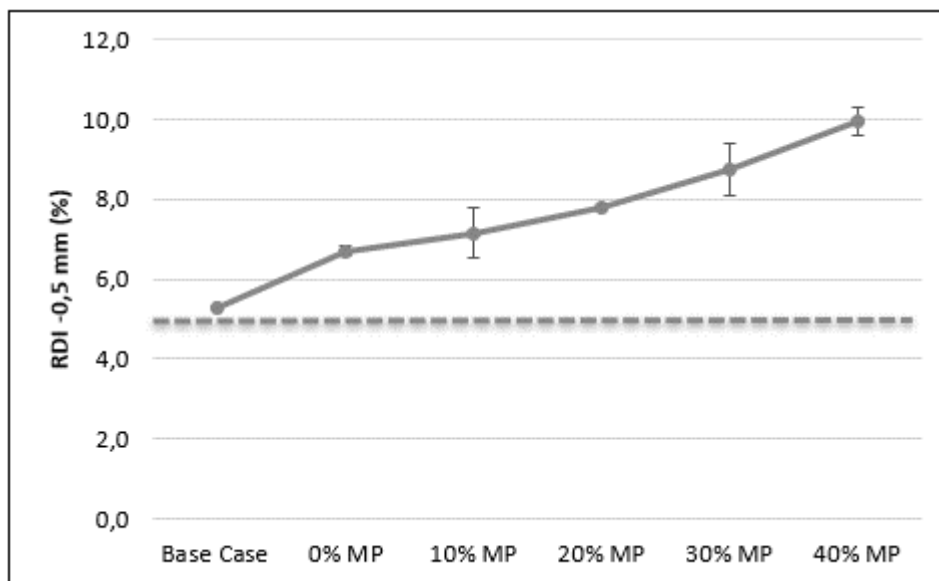
Figure 14: Impact of micropellet and concentrate addition on -0.5 mm reduction disintegration index. (Maximum industry allowed value of 5% indicated on the diagram.)
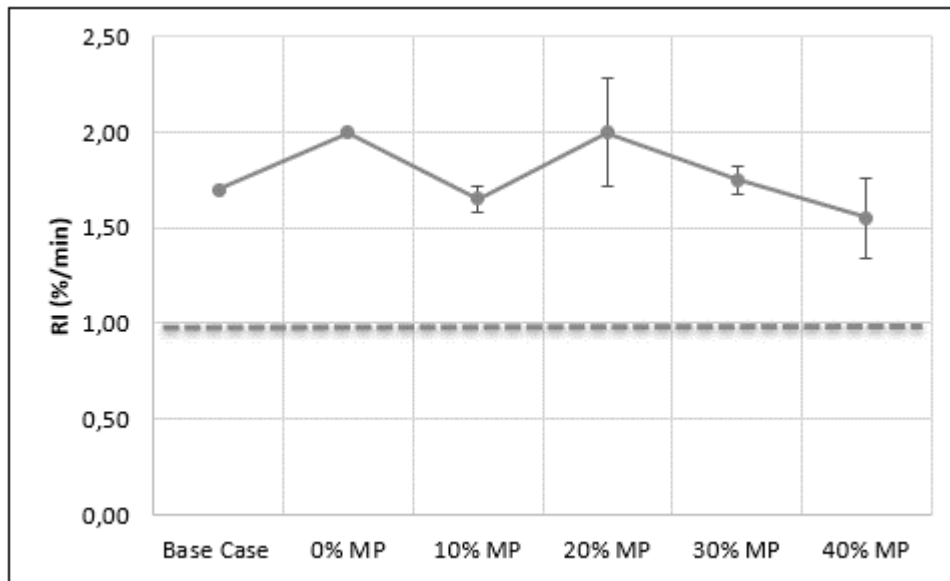
Figure 15: The impact of micropellet and concentrate addition on the
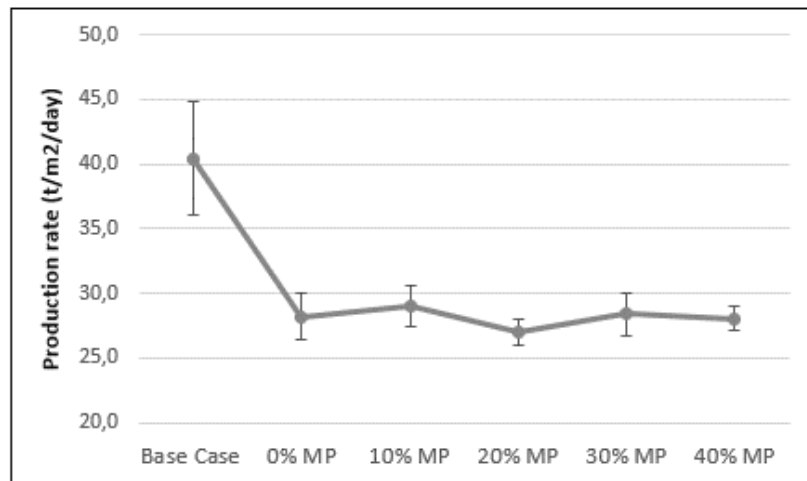reducibility index. (Minimum industry required value of 1%/min indicated on the
diagram.)

Figure 16: The influence of micropellet and concentrate addition on the production rate.

Figure captions:

Figure 1: Experimental setup for the measuring of the JPU (Nyembwe et al,.2016).

Figure 2. Schematic representation of the sinter pot test setup utilized at Anglo American Value-In-Use.

Figure 3: Maximum permeability as a function of micropellet to concentrate ratio. (Absence of error bars for some of the data points is due to little variability in the data.)

Figure 4. Mean granule size before ($D_{(BG)}$) and after ($D_{(AG)}$) granulation as a function of micropellet and concentrate content.

Figure 5. Material transfer (S) as a function of micropellet to concentrate ratio.

Figure 6: X-ray tomogram of micropellets obtained from the 30% MP mixture at 5.25% moisture.

Figure 7: Optical micrographs of iron ore concentrate and micropellets. a) Unreacted micropellet; b) Fired micropellet; c) Micropellet fired with fluxes.

Figure 8: Backscatter electron image of an iron ore micropellet obtained from the 20% MP sinter mixture showing a sintered layer surrounding an unreacted core

Figure 9: Cross sections of +16 mm sinter particles, reconstructed using MF-XRT. a) Base case; b) 0% MP; c) 10% MP; d) 20% MP; e) 30% MP; f) 40% MP.

Figure 10: Optical micrographs of the base case sinter. a) Attachment of bonding phase to the relict particle; b) Bonding phase structure.

Figure 11: The relative proportions of the crystalline sinter phases formed in the different sinter mixtures.

Figure 12: Tumble index as a function of concentrate and micropellet content.

Figure 13: Impact of micropellet and concentrate addition on -3.15 mm disintegration index.

Figure 14: Impact of micropellet and concentrate addition on -0.5 mm disintegration index. (Maximum industry allowed value of 5% indicated on the diagram.)

Figure 15: The impact of micropellet and concentrate addition on the reducibility index.

Figure 16: The influence of micropellet and concentrate addition on the production rate.